Micelles of Imidazolium-Functionalized Polystyrene Diblock Copolymers Investigated with Neutron and Light Scattering

Cheryl M. Stancik,[†] Adrien R. Lavoie,[‡] Jan Schütz,[‡] Paulina A. Achurra,[†] Peter Lindner,[§] Alice P. Gast,[||] and Robert M. Waymouth*,[‡]

Department of Chemical Engineering, Stanford University, Stanford, California 94305, Department of Chemistry, Stanford University, Stanford, California 94305, Institut Laue-Langevin, 156 Avenue des Martyrs, F-38042 Grenoble, Cedex 9, France, and Department of Chemical Engineering, Massachusetts Institute of Technology, Cambridge, Massachusetts 02139

Received July 25, 2003. In Final Form: October 16, 2003

We synthesize a series of block copolymers comprising a polystyrene (PS) block and an imidazolium-functionalized PS (IL) block and characterize their assembly properties. We use small-angle neutron scattering and dynamic light scattering to determine the micelle size and shape in dilute solutions and to assess the micelle interactions in concentrated solutions. By studying a series of copolymers with fixed PS block length, we find that the length of the IL block governs the micelle dimensions. Our data suggest that these copolymers form elongated micelle structures where the IL block is extended in the micelle core. We find that these micelles can sequester water and that interactions between the micelles lead to structure factor peaks at elevated concentrations.

I. Introduction

Self-assembly is a fundamental process in nature that is essential to life. As phospholipids are nature's building blocks to self-assembled materials, scientists have turned to block copolymers due to the ability to tune these systems through choice of monomer composition, molecular weight, and block architecture. As a consequence, copolymer micelles represent a rich and diverse class of materials that have promise in such applications as drug delivery,[1] flow modification,[2] catalysis,[3−6] and advanced materials.[7,8]

Under certain conditions of solvent, temperature, concentration, and composition, block copolymers will self-assemble into micelles to minimize their overall free energy. While the formation of block copolymer micelles in selective solvents greatly reduces the conformational entropy of the polymer system, these structures allow for the favorable contacts between the solvent and the block it solvates while minimizing the unfavorable interactions between the core-forming block and the solvent. The structure of the micelles created by the assembling copolymers adopts the appropriate geometry and packing to allow for the optimal balance between solvation of the chains of the micelle shell and protection of the insoluble core from the solvent environment. To exploit the unique and varied features of block copolymer micelles, we require a deeper understanding of how the self-assembly phenomenon of micelles is influenced by the architecture of the copolymer blocks they comprise.

In self-assembling systems, a variety of factors contribute to the geometry of the assemblies that form. Phenomenological models have predicted that the assembly process is driven by optimization of the interfacial areas of the core- and shell-forming blocks of an assembly and packing constraints.[9] In some systems, optimization of these constraints favors the formation of elongated structures denoted wormlike or rodlike micelles. These elongated micelle structures have been observed in many small-molecule surfactant systems using scattering, rheology, and microscopy and have been studied for decades due to their unique behavior and analogies to polyelectrolytes.[10,11]

Within the field of copolymer micelles, the relationships between copolymer composition and architecture and their assemblies have been considered.[12−18] The effect of block

* Corresponding author. Phone: (650) 723-4515. E-mail: waymouth@stanford.edu.
[†] Department of Chemical Engineering, Stanford University.
[‡] Department of Chemistry, Stanford University.
[§] Institut Laue-Langevin.
[||] Department of Chemical Engineering, Massachusetts Institute of Technology.

(1) Yang, L.; Alexandridis, P. *Curr. Opin. Colloid Interface Sci.* **2000**, *5*, 132−143.
(2) Bhatia, S. R.; Mourchid, A.; Joanicot, M. *Curr. Opin. Colloid Interface Sci.* **2001**, *6*, 471−478.
(3) Klingelhöfer, S.; Heitz, W.; Greiner, A.; Oestreich, S.; Förster, S.; Antonietti, M. *J. Am. Chem. Soc.* **1997**, *119*, 10116−10120.
(4) Bönnemann, H.; Richards, R. M. *Eur. J. Inorg. Chem.* **2001**, 2455−2480.
(5) Gupte, A.; Nagarajan, R.; Kilara, A. *Biotechnol. Prog.* **1991**, *7*, 348−354.
(6) Gupte, A.; Nagarajan, R.; Kilara, A. *Ind. Eng. Chem. Res.* **1995**, *34*, 2910−2922.
(7) Hedrick, J. L.; Miller, R. D.; Hawker, C. J.; Carter, K. R.; Volksen, W.; Yoon, D. Y.; Trollsås, M. *Adv. Mater.* **1998**, *10*, 1049−1053.
(8) Raez, J.; Barjovanu, R.; Massey, J. A.; Winnik, M. A.; Manners, I. *Angew. Chem., Int. Ed.* **2000**, *39*, 3862−3865.
(9) Israelachvili, J. N. *Intermolecular and Surface Forces*; Academic Press: London, 1992.
(10) Walker, L. M. *Curr. Opin. Colloid Interface Sci.* **2001**, *6*, 451−456.
(11) Sommer, C.; Pedersen, J. S.; Egelhaaf, S. U.; Cannavacciuolo, L.; Kohlbrecher, J.; Schurtenberger, P. *Langmuir* **2002**, *18*, 2495−2505.
(12) Förster, S.; Zisenis, M.; Wenz, E.; Antonietti, M. *J. Chem. Phys.* **1996**, *104*, 9956−9970.
(13) Antonietti, M.; Heinz, S.; Schmidt, M.; Rosenauer, C. *Macromolecules* **1994**, *27*, 3276−3281.
(14) Moffitt, M.; Eisenberg, A. *Macromolecules* **1997**, *30*, 4363−4373.
(15) Pispas, S.; Hadjichristidis, N.; Potemkin, I.; Khokhlov, A. *Macromolecules* **2000**, *33*, 1741−1746.
(16) Willner, L.; Poppe, A.; Allgaieri, J.; Monkenbusch, M.; Lindner, P.; Richter, D. *Europhys. Lett.* **2000**, *51*, 628−634.
(17) Altinok, H.; Nixon, S. K.; Gorry, P. A.; Attwood, D.; Booth, C.; Kelarakis, A.; Havredaki, V. *Colloids Surf., B* **1999**, *16*, 73−91.

10.1021/la0353632 CCC: $27.50
Published on Web 12/30/2003

ratio on the resulting properties of the assemblies has identified two major classes of spherical micelle geometries including "crew-cut" and starlike micelles.[19] Recently, many novel phases of self-assembled block copolymers have been observed. Bates and co-workers have performed a series of elegant scattering and microscopy experiments on structures formed from aqueous solutions of poly(ethylene oxide) (PEO) copolymerized with either poly(butadiene) (PB) or poly(ethyl ethylene) (PEE).[20−23] By altering the copolymer composition, they created assembled structures assuming spherical, cylindrical (wormlike micelles), and bilayer geometries quantified with advanced microscopy techniques.[21] Cross-linking the self-assembled wormlike chains resulted in the formation of giant macromolecules. These suprastructures were found to exhibit viscoelastic properties differing dramatically from those of their un-cross-linked analogues.[20] Their most recent studies on these systems visualized a series of unique assembly structures that consist of cylindrical loops and spherical caps joined by Y-junctions.[22] In a system of polystyrene−poly(acrylic acid) copolymers, Eisenberg and Zhang observed nonspherical aggregates including rods, lamellae, and vesicles using microscopy.[24] Further studies by Eisenberg and co-workers on a variety of other polystyrene-based block copolymer systems investigated the effects of polymer composition on crew-cut micelle structures[19] and the effects of ionic strength on micelle morphology.[25] Winnik, Manners, and co-workers explored the assembly of organometallic block copolymers of poly(ferrocenylsilane) with poly(dimethylsiloxane) and found altering the micelle preparation procedures resulted in either spherical or rodlike micelles as seen by microscopy.[26,27]

Here we present our findings on a series of imidazolium-functionalized polystyrene diblock copolymers. These copolymers comprise a homopolymer of polystyrene (PS) copolymerized with a PS block functionalized with an imidazolium cation (3-methylimidazolium) that we denote as the IL block. Many imidazolium cations belong to a class of materials called room temperature ionic liquids. This class of materials possesses the interesting property that while they are comprised entirely of ions, they are liquids at room temperature and over a wide temperature range often spanning 300 °C.[28] Ionic liquid solvents are interesting alternatives to conventional organic solvents; they may offer different selectivities and reactivity as reactive media. In addition, their low vapor pressure offers potential environmental benefits relative to conventional organic solvents.[29] The compatibility of ionic liquids with a range of both organic and inorganic materials allows diverse combinations of materials to come into a single phase making them attractive for traditional catalysis[29−31] as well as biocatalysis.[32,33] Incorporation of ionic liquid functionalities into well-defined polymer materials has only recently been explored.[34,35] Simmons and co-workers have prepared polymers that contain the imidazolium functionality with methacrylate-based monomers.[34,35] They assessed the polymer's ability to catalyze a hydrolysis reaction under varying conditions of pH, polymer and substrate concentrations, and polymer molecular weight.[35] As diblocks, our imidazolium-functionalized copolymers assemble into small micelle domains where their reactivity can be altered to meet specific needs.

In our initial study of these novel copolymers, we present their synthesis and characterize their micelle assemblies. Through our study of imidazolium-functionalized PS diblock copolymers, we aim to elucidate relationships between the architecture of the diblocks and the properties of their assemblies. In this work, we consider the effect of the length of the imidazolium-functionalized block on the micelle assemblies. Small-angle scattering techniques have been employed extensively in the study of block copolymer micelles and have been the subject of recent reviews.[36,37] Here we employ scattering techniques, including small-angle neutron scattering (SANS) and dynamic light scattering (DLS), to characterize the micelle properties including the single micelle size and shape as well as the intermicelle interactions.

II. Experimental Section

II.1. Copolymer Synthesis and Characterization. A series of imidazolium-functionalized block copolymers were generated from a polystyrene−poly(chloromethyl styrene) (PS−PCMS) copolymer precursor created by the nitroxide-mediated free-radical polymerization of styrene and chloromethyl styrene (CMS).[38−40] Reaction of the PS−PCMS precursor copolymer with 1-methylimidazole led to the conversion of the PCMS block into a charged block with imidazolium ionic liquid functionalities that we denote the IL block. Thus, the PS−IL copolymers comprise a PS block and an imidazolium-functionalized PS block. The general synthetic procedure with the structures of the products and intermediates is shown in Scheme 1. The PS−IL products contain a chloride counterion unless counterion exchange was performed with sodium tetrafluoroborate ($NaBF_4$) to generate a BF_4^- counterion.

II.1.a. Synthetic Procedures. All synthetic manipulations were carried out using standard Schlenk techniques under an inert atmosphere. Reagent grade *N*,*N*-dimethylacetamide (Aldrich) was degassed with three freeze−pump−thaw cycles prior to use. $NaBF_4$, 1-methylimidazole, styrene, CMS, xylenes, and toluene were obtained from Aldrich, and all were used without further purification. 1-Ethyl-3-methylimidazolium chloride (99+%)

(18) Burguière, C.; Pascual, S.; Bui, C.; Vairon, J. P.; Charleux, B.; Davis, K. A.; Matyjaszewski, K.; Bétremieux, I. *Macromolecules* **2001**, *34*, 4439−4450.
(19) Moffitt, M.; Khougaz, K.; Eisenberg, A. *Acc. Chem. Res.* **1996**, *29*, 95−102.
(20) Won, Y. Y.; Davis, H. T.; Bates, F. S. *Science* **1999**, *283*, 960−963.
(21) Won, Y. Y.; Brannan, A. K.; Davis, H. T.; Bates, F. S. *J. Phys. Chem. B* **2002**, *106*, 3354−3364.
(22) Jain, S.; Bates, F. S. *Science* **2003**, *300*, 460−464.
(23) Won, Y. Y.; Davis, H. T.; Bates, F. S.; Agamalian, M.; Wignall, G. D. *J. Phys. Chem. B* **2000**, *104*, 7134−7143.
(24) Zhang, L. F.; Eisenberg, A. *Science* **1995**, *268*, 1728−1731.
(25) Zhang, L. F.; Yu, K.; Eisenberg, A. *Science* **1996**, *272*, 1777−1779.
(26) Massey, J.; Power, K. N.; Manners, I.; Winnik, M. A. *J. Am. Chem. Soc.* **1998**, *120*, 9533−9540.
(27) Massey, J. A.; Temple, K.; Cao, L.; Rharbi, Y.; Raez, J.; Winnik, M. A.; Manners, I. *J. Am. Chem. Soc.* **2000**, *122*, 11577−11584.
(28) Wasserscheid, P.; Keim, W. *Angew. Chem., Int. Ed.* **2000**, *39*, 3772−3789.
(29) Rogers, R. D.; Seddon, K. R. *Ionic liquids*: *Industrial Applications to Green Chemistry*; American Chemical Society: Washington, DC, 2002; Vol. 818.
(30) Sheldon, R. *Chem. Commun.* **2001**, 2399−2407.
(31) Welton, T. *Chem. Rev.* **1999**, *99*, 2071−2083.
(32) van Rantwijk, F.; Lau, R. M.; Sheldon, R. A. *Trends Biotechnol.* **2003**, *21*, 131−138.
(33) Sheldon, R. A.; Lau, R. M.; Sorgedrager, M. J.; van Rantwijk, F.; Seddon, K. R. *Green Chem.* **2002**, *4*, 147−151.
(34) Simmons, M. R.; Patrickios, C. S. *Macromolecules* **1998**, *31*, 9075−9077.
(35) Patrickios, C. S.; Simmons, M. R. *Colloids Surf., A* **2000**, *167*, 61−72.
(36) Pedersen, J. S.; Svaneborg, C. *Curr. Opin. Colloid Interface Sci.* **2002**, *7*, 158−166.
(37) Castelletto, V.; Hamley, I. W. *Curr. Opin. Colloid Interface Sci.* **2002**, *7*, 167−172.
(38) Hawker, C. J.; Bosman, A. W.; Harth, E. *Chem. Rev.* **2001**, *101*, 3661−3688.
(39) Kazmaier, P. M.; Daimon, K.; Georges, M. K.; Hamer, G. K.; Veregin, R. P. N. *Macromolecules* **1997**, *30*, 2228−2231.
(40) Lacroix-Desmazes, P.; Delair, T.; Pichot, C.; Boutevin, B. *J. Polym. Sci., Part A*: *Polym. Chem.* **2000**, *38*, 3845−3854.

Scheme 1. Typical Synthetic Protocol for the Generation of PS−IL Block Copolymers

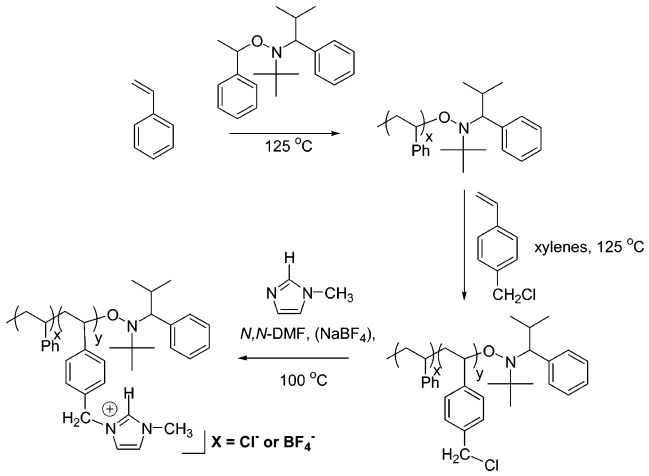

Table 1. Synthetic Properties of the PS−IL Block Copolymers and Their PS−PCMS Precursors

diblock copolymer	PS block			PS−PCMS		IL block	
	dp[a,b]	PDI[b,c]	M_n[b]	PDI[b,c]	M_n[d]	dp[a,d]	X[e]
PS(160)−IL(15)	160	1.10	16 600	1.13	18 900	15	Cl^-
PS(197)−IL(13)	197	1.05	20 400	1.11	22 400	13	Cl^-
PS(198)−IL(44)	198	1.05	20 600	1.06	27 500	44	BF_4^-
PS(198)−IL(75)	198	1.05	20 600	1.05	32 200	75	BF_4^-
PS(198)−IL(111)	198	1.05	20 600	1.10	37 700	111	BF_4^-

[a] Degree of polymerization. [b] As determined using GPC calibrated with linear PS standards. [c] Polydispersity index. [d] As determined by ^{1}H NMR. [e] Imidazolium counterion.

was obtained from Acros Organics. The initiator, 2,2,5-trimethyl-3-(1-phenylethoxy)-4-phenyl-3-azahexane, was prepared according to a literature procedure.[38,41]

Synthesis of PS. A 10 mL ampule was charged with 2,2,5-trimethyl-3-(1-phenylethoxy)-4-phenyl-3-azahexane (0.84 mol %) and styrene along with a small stir bar. The ampule was freeze−pump−thaw degassed (3×) and flame-sealed under nitrogen. The ampule was then suspended in a preheated oil bath (125 °C) for 8 h followed by cooling to ambient temperature. Once cooled, the resultant material was dissolved in CH_2Cl_2 (1 mL) and was added dropwise to CH_3OH (300 mL) with vigorous stirring. The slurry was stirred for 8 h followed by isolation on a glass frit. This precipitation procedure was repeated, and the resultant white solid was evaporated under reduced pressure. Polydispersities of PS products were determined by gel permeation chromatography (GPC) analysis against linear PS standards. The PS products had narrow molecular weight distributions with typical polydispersity indexes of 1.05−1.10. Characterization data for the PS blocks are shown in Table 1.

Synthesis of PS−PCMS. A PS polymer of the desired molecular weight was prepared using the procedure described above and was subsequently used in this reaction. An ampule was charged with the PS, CMS, xylenes, and a small stir bar. While the ratio of PS to CMS was held constant at 1:10 by weight, the amount of xylenes was adjusted to alter the copolymerization kinetics, thus allowing for controllable polymerization conditions and block ratios. The ampule was freeze−pump−thaw degassed (3×) and flame-sealed under nitrogen before suspension in a preheated oil bath (125 ° C) for 0.5 h. After cooling, the yellow material was dissolved in CH_2Cl_2 (3 mL) and was precipitated via dropwise addition to a vigorously stirred beaker of CH_3OH (300 mL). The slurry was stirred for 8 h followed by isolation on a glass frit. This precipitation procedure was repeated, and the resultant white solid was evaporated under reduced pressure. The degree of monomer incorporation was determined using ^{1}H NMR ($CDCl_3$) spectroscopy by integration of the ortho aromatic protons of the PS and PCMS versus the benzylic PCMS protons.

Typical Derivatization of PS−PCMS with 1-Methylimidazole. A Schlenk flask was charged with the PS−PCMS product prepared as described earlier (350 mg), 1-methylimidazole (2.3 mL, 28.0 mmol), and dry *N,N*-dimethylacetamide (10 mL). In addition, $NaBF_4$ (306 mg, 2.8 mmol) was added to the flask when exchange of the chloride counterion for BF_4^- was desired. The solution was heated at 100 °C for 7 h followed by cooling to ambient temperature. The solvent was removed under reduced pressure followed by the addition of water (3 mL) with stirring for 8 h. The off-white solid was isolated on a glass frit followed by reprecipitation and isolation. The resultant solid was evaporated under reduced pressure in a 40 °C oil bath for 2 days. We denote the products of the derivatization reactions as PS−IL, and a summary of the prepared polymers is found in Table 1.

II.1.b. Characterization of Copolymer Products and Precursors. A summary of the characterization data for the PS−IL block copolymer precursors and the properties of the final PS−IL diblocks is given in Table 1. Deuterated DMSO (D_6, Cambridge Isotopes Laboratories, D 99.9%) and chloroform (D_1, Cambridge Isotopes Laboratories, D 99.8%) were used without further purification. ^{1}H NMR spectra were recorded on a Varian 400 MHz spectrometer, and $^{13}C\{^1H\}$ NMR spectra were recorded on a Varian UI300 spectrometer operating at 75.4 MHz. Chemical shifts are reported in ppm relative to residual solvent resonances (^{1}H). GPC analyses were conducted with a Millipore model 510 instrument equipped with Styragel HR columns. Polydispersities of the PS−PCMS products were determined by GPC analysis against linear PS standards.

Typical ^{1}H NMR Characterization of PS−PCMS. (1) PS(198)−PCMS(111). ^{1}H NMR (400 MHz, 300 K, $CDCl_3$, δ): 7.25−6.90 (7.4 H, m, Ar-*H meta* + *para*), 6.70−6.30 (5.6 H, m, Ar-*H ortho*), 4.51 (2.0 H, s, CH_2Cl), 2.10−1.20 (8.3 H, m, CH_2CH). The relative proton integrals vary between the different polymers according to the respective block lengths. The number of repeat units of CMS was evaluated from the integration of the benzyl chloride protons (CH_2 of CMS block) and comparison with the sum of the integrals for all ortho aromatic protons. This ratio in combination with GPC (M_n) data allowed for determination of the relative block lengths.

$^{13}C\{^1H\}$ NMR (75.4 MHz, 300 K, $CDCl_3$, δ): 146.5−145.0, 134.9, 129.0−127.0, 125.8, 46.3, 43.8, 41.0−40.0. We note that resonances corresponding to the various carbon nuclei were broad and were not completely differentiated in this spectrum, and as such, ranges for these resonances have been reported which correspond to various inequivalent nuclei.

(2) Elemental Analyses. Typical PS−PCMS copolymer samples were analyzed by elemental analysis, and results are shown as follows where all values are given as percentages. PS(197)−PCMS(13) Anal. Calcd: C, 90.28; H, 7.56. Found: C, 90.06; H, 7.61. PS(198)−PCMS(44) Anal. Calcd: C, 86.93; H, 7.32; N, 0.05. Found: C, 87.32; H, 7.31; N, <0.05. PS(198)−PCMS(75) Anal. Calcd: C, 84.58; H, 7.12; N, 0.04. Found: C, 84.63; H, 7.13; N, <0.05. PS(198)−PCMS(111) Anal. Calcd: C, 82.58; H, 6.95; N, 0.03. Found: C, 82.59; H, 6.89; N, <0.05.

Typical Characterization of PS−IL. (1) PS(198)−IL(111). ^{1}H NMR (400 MHz, 300 K, d_6-DMSO, δ): 9.20 (1.0 H, s, N=C*H*N), 8.25−6.10 (12.9 H, m, Ar-*H* and *H*CN=CN*H*), 5.35 (2.0 H, s, CH_2), 3.97 (3.0 H, s, NCH_3), 2.20−0.80 (8.4 H, m, CH_2CH). We note that the relative number of protons varies between the different polymers according to the respective block lengths.

$^{13}C\{^1H\}$ NMR (75.4, 300 K, d_6-DMSO, δ): 146.0−145.0, 136.3, 131.8, 128.2, 124.1, 123.3, 51.7, 35.8. We again note that resonances corresponding to the various carbon nuclei were broad and were not completely differentiated in this spectrum, and as before, we report ranges for these resonances, which correspond to various inequivalent nuclei.

(2) Elemental Analysis. Elemental analysis was performed on typical PS−IL samples, and the results are shown below where all values are given as percentages. These results indicate nearly quantitative conversion of the PCMS to IL and that the desired structures were achieved. In all cases, when performed the counterion exchange (Cl^- to BF_4^-) was nearly quantitative (>98%). PS(197)−IL(13) Anal. Calcd: C, 88.91; H, 7.55; N, 1.53;

(41) Benoit, D.; Chaplinski, V.; Braslau, R.; Hawker, C. J. *J. Am. Chem. Soc.* **1999**, *121*, 3904−3920.

Cl, 1.94. Found: C, 89.39; H, 7.49; N, 1.52; Cl, 1.94. PS(198)−IL(44) Anal. Calcd: C, 78.01; H, 6.84; N, 3.72; Cl, 0.00. Found: C, 77.84; H, 7.05; N, 3.47; Cl, 0.12. PS(198)−IL(75) Anal. Calcd: C, 73.11; H, 6.51; N, 4.99; Cl, 0.00. Found: C, 73.56; H, 6.37; N, 4.46; Cl, 0.06. PS(198)−IL(111) Anal. Calcd: C, 69.49; H, 6.27; N, 5.93, Cl, 0.00. Found: C, 69.37; H, 6.10; N, 5.54; Cl, 0.10.

II.2. Copolymer and Micelle Scattering. *Scattering Sample Preparation.* Dilute solutions of the diblock copolymers were prepared at 0.70 wt % by mass in the chosen solvent. For one diblock, PS(198)−IL(111), concentrated samples were prepared at 5 and 20 wt % in addition to the dilute solution. Hydrogenated solvents used for DLS included methanol and toluene (J. T. Baker). Deuterated toluene (D_8, Cambridge Isotopes Laboratories, D 99.6%) was used for the SANS experiments. All solvents were used as received for the preparation of the scattering samples unless noted. Samples were allowed to equilibrate overnight and were studied within a few days of preparation. Some samples required stirring and mild heating to achieve complete dissolution. Once dissolution had been achieved, all solutions were clear and most were colorless while a few exhibited a faint blue hue characteristic of colloidal solutions.

DLS Data Collection and Analysis. DLS experiments allowed determination of the hydrodynamic radii, R_h, of the diblock copolymer micelles. Sample vials were thoroughly cleaned and rinsed with filtered solvent. To ensure samples were free of dust, each sample was prepared with filtered solvent and passed through a 0.2 μm inorganic membrane filter (Whatman Anotop) directly into the scattering vial. The DLS experiments were conducted using a Coherent DPSS 500 mW laser at a wavelength of 532 nm. For each sample, the laser was attenuated as needed and the data were collected at seven scattering angles from 30 to 150° in 20° steps. This scattering angle (θ) is related to the momentum transfer, q, defined as $q = (4\pi/\lambda)\sin(\theta/2)$ where λ is the wavelength of light in the medium. All data were taken at a fixed temperature of 25 °C maintained by a circulating temperature bath. Autocorrelation data were obtained from the DLS experiments using an ALV/DLS/SLS-5000 instrument with ALV-5000/E/WIN Multiple τ Digital Realtime Correlator Software. Analysis was performed with the ALV-NonLin data analysis routine that uses a constrained regularization method which fits an integral type model function to the autocorrelation data to give values of the decay time, τ. This analysis procedure is analogous to the CONTIN methods given by Provencher.[42]

For our samples, the analysis yielded a single dominant τ indicating a unimodal distribution of particles. The inverse of τ is the decay rate, Γ, and can be related to the translational diffusion coefficient of the particles, D_T, through the expression $\Gamma = D_T q^2$. Hence, a plot of Γ versus q^2 should yield a line with a slope equal to D_T. Plots of our data showed excellent linearity with intercepts of nearly zero. By approximating the particles as effective, noninteracting spheres, we can employ the Stokes−Einstein relationship ($D_T = kT/(6\pi\eta R_h)$), to obtain R_h, where k is the Boltzmann constant, T is the temperature, and η is the solvent viscosity.

SANS Data Collection. SANS experiments of the diblock copolymers and their micelles allowed for a detailed analysis of the micelle structures. Scattering experiments were performed on the 80 m instrument (D11) at Institut Laue-Langevin (ILL) (Grenoble, France) and the 30 m instrument (NG3) at the National Institute of Standards and Technology (NIST) Center for Cold Neutron Research (Gaithersburg, MD). For each experiment, the sample-to-detector (S−D) distance was chosen in order to obtain the desired range of the momentum transfer, q. For all SANS experiments, the temperature was maintained at 25 °C.

SANS experiments on copolymers PS(160)−IL(15), PS(160)−CMS(15), and PS(197)−IL(13) were performed at ILL with a wavelength of $\lambda = 6$ Å with a wavelength spread of $\Delta\lambda/\lambda = 0.09$. All the samples were studied at two S−D distances of 3.0 and 10.0 m to obtain a q-range of 0.0054−0.1200 Å^{-1}. An additional S−D distance of either 17.0 or 36.7 m was used for the micelle solutions to extend the q-range with a minimum q-value of either 0.0031 or 0.0026 Å^{-1}, respectively. Samples were contained in 1 mm quartz cells (Hellma, 404-QS) with Teflon caps to prevent loss of solvent. The two-dimensional intensity data were corrected and radial averaging was performed to obtain one-dimensional absolute scattering intensity data using correction and reduction routines developed at ILL.[43]

SANS experiments on copolymers PS(198)−IL(75) and PS(198)−IL(111) and their precursors were performed at NIST at a wavelength of $\lambda = 6$ Å and, for some samples, 8 Å, with a wavelength spread of $\Delta\lambda/\lambda = 0.150$. Copolymers PS(198)−CMS(75) and PS(198)−CMS(111) were studied at a S−D distance of 13.1 m with 6 Å neutrons giving a q-range of 0.0046−0.0450 Å^{-1}. For samples PS(198)−IL(75) and PS(198)−IL(111), three S−D distances of 1.3, 5.0, and 13.1 m were used where the detector was offset from center 20 cm at the shortest S−D distance to give a larger q-range. For the 1.3 and 5.0 m distances, 6 Å neutrons were used, while a special configuration employing lenses was used at 13.1 m with 8 Å neutrons to extend the low-q range.[44] These three configurations allowed for a q-range of 0.0001−0.4300 Å^{-1}. Samples were contained in 1 mm cells with quartz windows provided by NIST. The two-dimensional intensity data were corrected and averaged to obtain one-dimensional data on an absolute scale using data correction and reduction routines developed at NIST.[45]

SANS Data Analysis. The contribution to the scattering intensity due to the sample cell is removed from the one-dimensional data using the reduction procedures provided by the scattering facilities. Solvent scattering contributes to the profile as a uniform background and can be subtracted on a volume fraction basis. For a solution of identical particles, the macroscopic differential scattering cross section, $d\Sigma/d\Omega$ (q), can be expressed as follows.[46]

$$\frac{d\Sigma}{d\Omega}(q) = (\Delta\rho)^2 N V^2 P(q) S(q) + B \qquad (1)$$

In this expression, $(\Delta\rho)^2$ is the neutron contrast, N is the number density of scattering centers, V is the volume of a scattering center, $P(q)$ and $S(q)$ are the form and structure factors, respectively, and B is the incoherent background. The neutron contrast is defined as the square of the difference in the scattering length densities (SLD), ρ_i, of two components. For example, for components A and B, $(\Delta\rho)^2$ is equal to $(\rho_A - \rho_B)^2$. In our study, the contrast arises due to the difference in SLD of the hydrogenated polymers and the deuterated solvent. The form factor, $P(q)$, contains contributions to the scattering intensity due to interference effects within an individual scattering center and therefore gives information about the size and shape of the scattering centers. Analytical expressions have been developed for many common shapes, and we will employ some of these expressions to characterize our data. The structure factor, $S(q)$, arises from interference effects between different scattering centers and provides information about the interaction potential and local organization of scattering centers. When a solution is dilute, no interactions occur between scattering centers (or these interactions are sufficiently weak) such that $S(q)$ is unity over the entire q-range. Thus, in the case of our dilute solution studies, we do not consider the effects of the structure factor on the scattering profiles. The incoherent scattering, given by B, gives no structural information about the sample and is treated as a uniform background contribution to the scattering intensity.

From the low-q scattering data, we can determine the micelle radius of gyration (R_g). Due to the length scales of the structure probed by the low-q scattering regime, we can

(42) Provencher, S. W.; Hendrix, J.; De Maeyer, L.; Paulussen, N. *J. Chem. Phys.* **1978**, *69*, 4273−4276.

(43) Ghosh, R. E.; Egelhaaf, S. U.; Rennie, A. R. *A Computing Guide for Small-Angle Scattering Experiments*; Institut Max von Laue Paul Langevin: Grenoble, France, 2000.

(44) Choi, S. M.; Barker, J. G.; Glinka, C. J.; Cheng, Y. T.; Gammel, P. L. *J. Appl. Crystallogr.* **2000**, *33*, 793−796.

(45) *SANS Data Reduction and Imaging Software*; Cold Neutron Research Facility, NIST: Gaithersburg, MD, 1996.

(46) King, S. M. In *Modern Techniques for Polymer Characterisation*; Pethrick, R. A., Dawkins, J. V., Eds.; John Wiley & Sons Ltd.: New York, 1999; pp 171−232.

approximate the micelle structure as a uniform sphere. We fit the data using the analytical expression for the form factor of a uniform sphere.[47]

$$P(q,R_g) = \left\{\frac{3[\sin(qR_g) - qR_g\cos(qR_g)]}{(qR_g)^3}\right\}^2 \quad (2)$$

When we perform the fit of our SANS data to eq 1, we use eq 2 as the form factor with R_g as a fitting parameter and allow the prefactor in eq 1 containing information about the neutron contrast, number density, and scattering center volume to be fit as well. This prefactor can be related to the molecular weight of the scattering center (MW). For the PS−PCMS precursor copolymers, R_g is sufficiently small ($R_g < q^{-1}$) such that we can use the Guinier approximation where the expression given for the form factor of a uniform sphere (eq 2) can be approximated as follows using a series expansion.[48]

$$P(q,R_g) \approx \exp\left(-\frac{(qR_g)^2}{3}\right) \quad (3)$$

Hence, a Guinier plot ($\ln[d\Sigma/d\Omega\,(q)]$ versus q^2) should be linear in the low-q limit with a slope of negative $R_g^2/3$ and an intercept that contains information about the MW. We use the MW values of the PS−PCMS copolymers to confirm the absolute scaling of the SANS data.

Karl Fischer Water Content Testing. Karl Fischer water content testing was performed by Galbraith Laboratories (Knoxville, TN). The Karl Fischer titration technique allows determination of trace amounts of water present in our system including that in the toluene, contained within the micelle, and bound to the polymer. Ambient samples for Karl Fischer water content testing were prepared in the same fashion as the scattering samples. Water-saturated samples were prepared by adding an excess of Milli-Q deionized water (∼50 μL water per gram of polymer solution) to ambient samples using a micropipet. Mild heating and agitation were applied to the samples to facilitate the incorporation of the water. Once the sample became clear, the water-saturated polymer solution was removed from the excess water. The water-saturated samples remained clear with no evidence of polymer precipitation or phase separation.

III. Results and Discussion

III.1. Assessing the Copolymer Materials and Micelle Formation. The synthesis of the imidazolium-functionalized PS−IL block copolymers was carried out in a three-step procedure. First, a PS macroinitiator was prepared from styrene using the Hawker−Braslau nitroxide.[38,41] Analysis of this material by GPC indicated narrow polydispersities (Table 1). This macroinitiator was then used to generate the PCMS block using nitroxide-mediated living free-radical techniques.[39,40] The analysis of the resultant PS−PCMS diblock copolymer by GPC and ^{1}H NMR allowed for the determination of the composition and molecular weight of the PCMS block (Table 1). Finally, the reaction of these PS−PCMS diblock copolymers with 1-methylimidazole in *N*,*N*-dimethylacetamide resulted in the clean substitution of the chloride functionality with the imidazole. Analysis of these PS−IL ionic block copolymers by ^{1}H NMR and microanalysis indicated that >98% of the CMS groups were converted to IL groups under these conditions. In the case of PS(198)−IL(44), PS(198)−IL(75), and PS(198)−IL(111), $NaBF_4$ was added during the functionalization step to yield the BF_4^- derivatives. Precipitation of the ionic block copolymers was carried out with water to afford the imidazolium-functionalized PS−IL diblock copolymers.

Table 2. Micelle Assembly Properties Obtained from SANS and DLS[a]

diblock copolymer	R_g (Å)	R_h (Å)
PS(160)−IL(15)	178	224
PS(197)−IL(13)	198	257
PS(198)−IL(44)	*b*	412
PS(198)−IL(75)	396	565
PS(198)−IL(111)	499	709

[a] All data obtained from 0.7 wt % toluene solutions. [b] Data not available.

With the structures verified, we can begin considering the properties of the PS−IL copolymers by assessing the capacity of the PS−IL copolymers to form micelles in various solvent systems. Based on our knowledge of the solubility of the individual blocks, we chose to study toluene as a selective solvent for the PS block and methanol as a selective solvent for the IL block. In both solvents, we observe the formation of micelles as indicated by the R_h values for PS(160)−IL(15) of 224 and 291 Å in toluene and methanol, respectively. As we would like to study micelles with the IL block as the core-forming block, we focus the remainder of our studies on toluene solutions of the copolymers.

For some of the PS−IL copolymers, we study their PS−PCMS precursors in toluene (where both PS and PCMS are soluble) to characterize the single-chain properties of the precursor copolymers. We find the PS−PCMS copolymers exhibit properties of typical linear polymers as indicated by their R_g values which are 40−70 Å depending on their MW. By characterizing these unassembled precursor chains, we can compare the MW of self-assembled systems to those of the unassembled chains.

III.2. Low-*q* Micelle Characterization. Due to the length scales probed in the low-q portion of the scattering profile, the scattering profiles follow the form factor of a sphere in this regime despite potential variations of the micelles from spherical structures outside of this low-q limit. Thus, our method to obtain the overall R_g is not biased by the shape of the micelle. We obtained good fits in the low-q regime to eq 2 for all the copolymers, and the parameters obtained from the analysis are given in Table 2.

The data show that the length of the IL block (number of IL repeat units, N_{IL}) dictates the structure of their micelles. We find that both R_h and R_g can be linearly related to N_{IL} for a fixed PS block length of ∼200 repeat units as shown in Figure 1 where the data are presented along with linear least-squares fits. These linear relations indicate that the PS shell thickness is constant through the series of copolymers studied and thus only the IL block length controls the micelle dimensions. This finding is unexpected over such a large range of block ratios. Typically, as the curvature of the core−shell interface of a copolymer micelle decreases (due to an increase in the core radius) the conformation of the chains forming the micelle coronae changes from starlike to that found in polymer brushes.[19,49] These changes in the shell conformation impact its thickness. The relatively constant PS shell thickness implies that the PS chain conformation does not dramatically change in this regime of block ratios. We will explore the nature of the PS chain conformation in further detail in the following section.

III.3. Elongated Micelle Structures. The presence of elongated micelle structures was evident in the scattering profiles of the PS−IL copolymers having the longest

(47) Higgins, J. S.; Benoit, H. C. *Polymers and Neutron Scattering*; Clarendon Press: Oxford, 1994.
(48) Glatter, O.; Kratky, O. *Small-Angle X-ray Scattering*; Academic Press: London, 1982.
(49) Vagberg, L. J. M.; Cogan, K. A.; Gast, A. P. *Macromolecules* **1991**, *24*, 1670−1677.

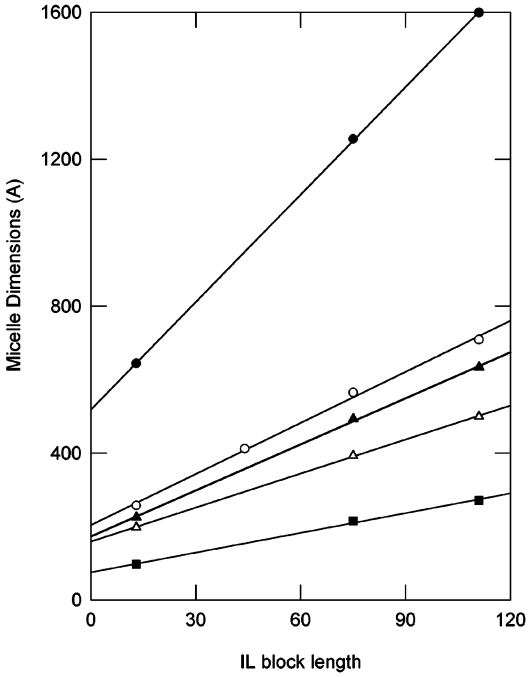

Figure 1. Micelle dimensions (L, closed circles; R_h, open circles; l_p, closed triangles; R_g, open triangles; $R_{g,xs}$, closed squares) obtained from DLS and the SANS Guinier and Kratky−Porod wormlike chain analyses of PS(197)−IL(13), PS(198)−IL(44), PS(198)−IL(75), and PS(198)−IL(111) plotted against the IL block length. The solid lines indicate least-squares fits to the data.

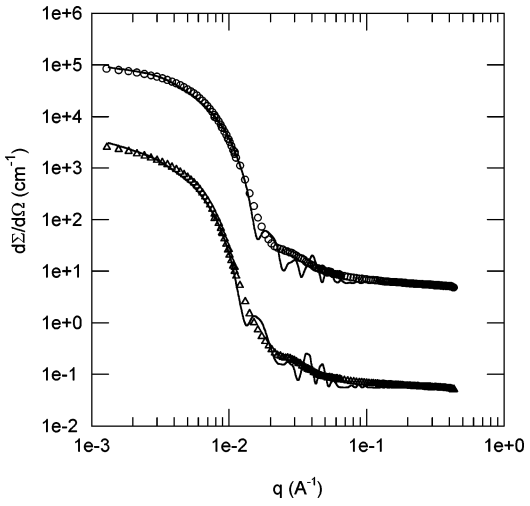

Figure 2. SANS scattering profiles are shown for PS(198)−IL(75) (open circles) and PS(198)−IL(111) (open triangles) at 0.7 wt % in toluene. The data for PS(198)−IL(75) have been offset by a factor of 100 for clarity. The core−shell cylinder model fits are indicated with a solid line. The solvent contribution to these scattering profiles has not been subtracted and is treated as a uniform background in the fitting procedure.

IL blocks shown in Figure 2. To investigate the potential presence of elongated structures, rodlike and wormlike chain analyses were applied for the copolymers with a fixed PS block length (∼200 repeat units) and varying IL block lengths with N_{IL} of 13, 75, or 111.

We initially began our SANS analysis applying a spherical core−shell form factor to the data. While we obtained a satisfactory fit of the PS(197)−IL(13) SANS profiles to the core−shell form factor, we found the micelle core radius had an unusually high polydispersity. Furthermore, the SANS profiles for the two copolymers with the longest IL blocks (PS(198)−IL(75) and PS(198)−IL(111)) did not follow the core−shell form factor over the entire q-regime; the initial decay linking the low- and intermediate-q regimes could not be reproduced with this model. This led us to consider that our micelles may be adopting nonspherical, elongated geometries. In these systems, as the IL block grows it may become difficult to pack the long linear chains into a spherical core. Hence, this steric packing constraint may favor elongated structures. This concept is analogous to that observed in the phase separation of diblock copolymers in the melt; as the block sizes become more equal, the morphology of the system changes from a cubic array of spheres to a lamellar structure.[50] As we can rationalize the motivation for the system to adopt nonspherical structures, we now turn to the scattering data to develop a more quantitative understanding of this phenomenon.

Table 3. Micelle Properties Obtained from the SANS Analyses

diblock copolymer	$R_{g,xs}$ (Å)	L (Å)	l_p (Å)
PS(197)−IL(13)	97	644	225
PS(198)−IL(75)	215	1255	493
PS(198)−IL(111)	271	1599	634

We first apply the Kratky−Porod wormlike chain model to the SANS data. In this approximation, the form factor for an infinitely thin needle is employed. We consider this expression in the intermediate-q regime and incorporate a Guinier-like factor to obtain an approximation for the form factor of a wormlike chain.[46]

$$\frac{d\Sigma}{d\Omega}(q) \approx \pi N V^2 (\Delta\rho)^2 \left(\frac{1}{qL}\right) \exp\left(-\frac{q^2 R_{g,xs}{}^2}{2}\right) + B \quad (4)$$

In this expression, L is the length of the wormlike chain and $R_{g,xs}$ is the radius of gyration of the wormlike chain cross section. For a wormlike chain, a plot of $\ln[q \times d\Sigma/d\Omega\,(q)]$ versus q^2 will show linear behavior in the appropriate q-regime with a slope (m) yielding $R_{g,xs}$ ($R_{g,xs} = (-2m)^{1/2}$). The data for all three copolymers are linear at intermediate q when plotted this way as shown in Figure 3 along with the linear least-squares fits to the data. The associated $R_{g,xs}$ values obtained from these fits are presented in Table 3. In the low-q regime, the scattering is due to the entire micelle structure, while the scattering in the high-q regime arises from the structure of the polymer chains comprising the micelles. Thus, it is between these two limits in the intermediate-q regime that the cross-sectional dimension of the wormlike micelle structure is observed.

Our data show that the $R_{g,xs}$ values of the three copolymers are linearly related to N_{IL}, and we summarize the data in Figure 1 with a linear least-squares fit. To understand the relationship between $R_{g,xs}$ and the IL block length, we consider the linear analysis in detail. The linear relation implies that the PS shell conformation does not depend on the IL block length for the range of block ratios considered. We evaluate the expression relating $R_{g,xs}$ to N_{IL} for an IL block of zero units, thus investigating the behavior of the PS shell. The expression predicts an $R_{g,xs}$ of 76 Å for a vanishing IL block, indicating the PS shell thickness. We employ the relationship describing the scaling behavior of linear polymer chains ($R_g = N_s{}^{\nu} a_s \times 6^{-1/2}$) where ν is the Flory exponent, a_s is the statistical segment length of the polymer, and N_s is the number of statistical units (i.e., the total number of monomer repeat units divided by the number of monomers per statistical segment). Using the statistical segment length found for

(50) Bates, F. S. *Science* **1991**, *251*, 898−905.

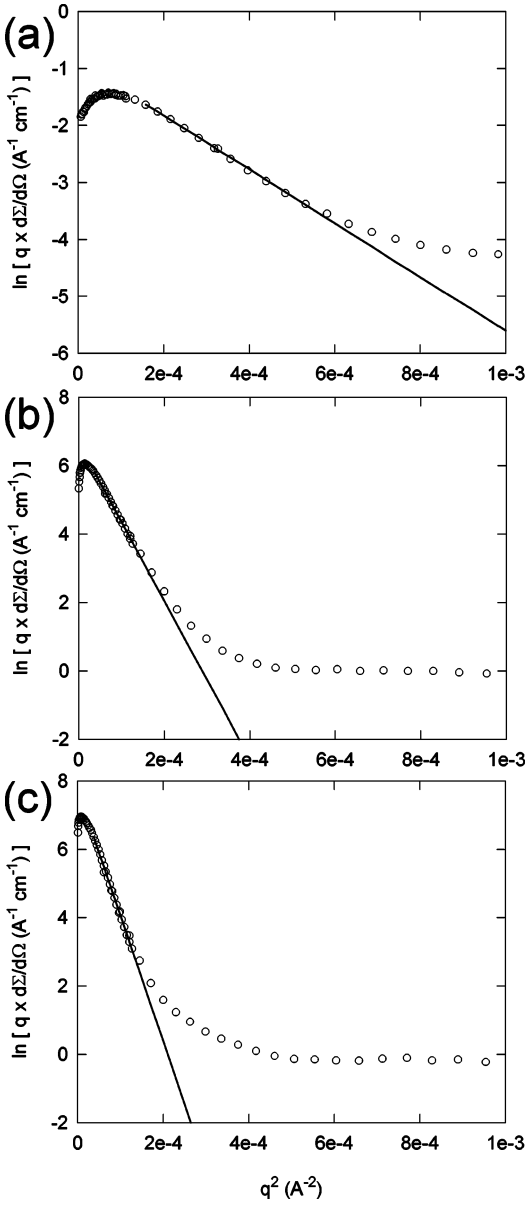

Figure 3. The Kratky−Porod wormlike chain analysis is shown for (a) PS(197)−IL(13), (b) PS(198)−IL(75), and (c) PS(198)−IL(111) at 0.7 wt % in toluene. The solid lines indicate the linear fits used to obtain the $R_{g,xs}$ of the elongated micelles.

linear PS of 15.5 Å,[51] we find ν adopts the value of a swollen polymer chain in a good solvent ($\nu = 0.57$) consistent with the behavior for a PS chain in toluene. The linear relation between $R_{g,xs}$ and N_{IL} suggests the polymer of the IL block is highly stretched approaching a fully extended conformation ($\nu = 1$). We anticipate stretched chains since the bulky nature of the ionomeric IL blocks favors extended chains as steric hindrance may prevent more coiled conformations. From the slope of the linear relation between $R_{g,xs}$ and N_{IL}, we find that $R_{g,xs}$ increases 1.8 Å per IL repeat unit. Thus, the cross-sectional diameter ($2R_{g,xs}$) increases by 3.6 Å per IL repeat unit which is essentially the IL repeat unit extended length (i.e., twice the carbon−carbon single bond length, 3.1 Å), indicating the extension of the IL block across the core of the micelle. This presence of highly stretched chains has interesting consequences on their ability to pack efficiently into micelle structures. While we initially suspected growing IL block

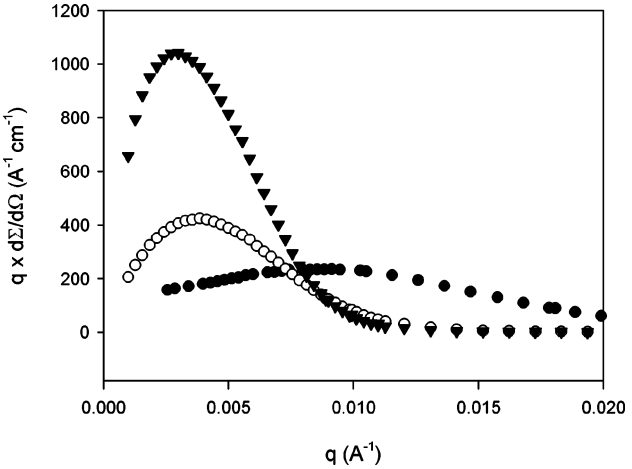

Figure 4. Bending rod plots are shown for PS(197)−IL(13) (closed circles), PS(198)−IL(75) (open circles), and PS(198)−IL(111) (closed triangles) at 0.7 wt % in toluene. The data for PS(197)−IL(13) have been multiplied by a factor of 1000.

length led to nonspherical structures, it appears that the inability of the extended IL blocks to pack efficiently into spherical structures favors elongated micelles for all IL block lengths. We find excellent linear agreement to the Kratky−Porod wormlike chain behavior for all three of the structures studied over a large range of block ratios.

Another signature of elongated structures is seen in a bending rod or Holtzer plot in which the flexibility of elongated structures can be characterized.[52] In this representation of dilute solution scattering data, a maximum in a plot of $q \times d\Sigma/d\Omega$ (q) versus q can be observed when the length of an elongated structure exceeds twice its persistence length ($L > 2l_p$).[53] This maximum occurs approximately at a q-value equal to $6/(\pi l_p)$, providing a measure of the micelle flexibility.[54] Our bending rod plots show a maximum as shown in Figure 4, and the associated l_p values are given in Table 3. Qualitatively, with growing IL block length the maximum becomes more pronounced and shifts to lower q. Quantitatively, we find that the IL block length dictates the structures as l_p and N_{IL} are linearly related as shown in Figure 1 with their linear least-squares fits. Thus, as the IL block length is increased, the elongated micelles become stiffer. This appears to be a consequence of the increased $R_{g,xs}$ consisting of fully extended IL chains, which seems to resist bending as it may disrupt the packing of the core.

As our Kratky−Porod wormlike chain and bending rod plot analyses indicate the rodlike nature of the micelle structures, we use the geometric relationship developed for a rod relating R_g to the cross-sectional rod radius (R_{xs}) and length (L).[47]

$$R_{g,rod}^2 = \frac{L^2}{12} + \frac{R_{xs}^2}{2} \qquad (5)$$

Since R_g and $R_{g,xs}$ are obtained from different q-regimes, they are independent measures of the micelle size. Thus, by approximating $R_{g,xs}$ as R_{xs} we can obtain the length of the micelle structures from eq 5 as given in Table 3 and see L is a linear function of the IL block length. The expression relating L to the IL block length indicates that

(51) Cogan, K. A.; Gast, A. P.; Capel, M. *Macromolecules* **1991**, *24*, 6512−6520.

(52) Denkinger, P.; Burchard, W. *J. Polym. Sci., Part B: Polym. Phys.* **1991**, *29*, 589−600.

(53) Magid, L. J.; Li, Z.; Butler, P. D. *Langmuir* **2000**, *16*, 10028−10036.

(54) Garamus, V. M.; Pedersen, J. S.; Maeda, H.; Schurtenberger, P. *Langmuir* **2003**, *19*, 3656−3665.

Table 4. Micelle Properties Obtained from Core−Shell Cylinder Fits

diblock copolymer	R_{core} (Å)	L (Å)	t_{shell} (Å)
PS(198)−IL(75)	153	1072	129
PS(198)−IL(111)	235	1770	137

with each additional IL unit added to the IL block, the wormlike chain grows about 10 Å.

To determine whether the scattering curve is consistent with an elongated micelle, we fit the data for PS(198)−IL(75) and PS(198)−IL(111) using a model describing a core−shell cylinder.[55] The scattering amplitude for a right cylinder of length L with a core cross-sectional radius R and uniform shell thickness t over the entire particle is

$$f(q,\alpha) = \frac{2(\rho_{core} - \rho_{shell})V_{core}\sin(qH\cos\alpha)J_1(qR\sin\alpha)}{(qH\cos\alpha)(qR\sin\alpha)} + \frac{2(\rho_{shell} - \rho_{solvent})V_{shell}\sin(q(H+t)\cos\alpha)J_1(q(R+t)r\sin\alpha)}{(q(H+t)\cos\alpha)(q(R+t)r\sin\alpha)} \quad (6)$$

In eq 6, $J_1(x)$ is the first-order Bessel function evaluated for x and α is the angle between q and the cylinder axis. Here, the volumes of the core and shell of the cylinder are simply evaluated from the geometry ($V_{core} = \pi r^2 L$ and $V_{shell} = \pi(R+t)^2(L+2t)$, respectively) and ρ_i denotes the SLD as defined previously. The form factor for the right cylinder, $P(q)_{cyl}$, is then given by

$$P(q)_{cyl} = \frac{\phi}{V_{shell}}\langle f^2\rangle \quad (7)$$

where ϕ is the volume fraction and the triangular brackets indicate that an orientational average is taken for $0 < \alpha < \pi/2$.

This model accurately characterizes the scattering curve over the entire range of q, indicating again that the data are consistent with elongated micelle structures as shown in Figure 2 where the fits are shown with the data. The parameters from these core−shell cylinder fits are given in Table 4. We find that the micelle dimensions from these fits are quite consistent with the data obtained from the low-q and Kratky−Porod wormlike chain analyses. Thus, all of our data and analyses support the conclusion of elongated micelles with an aspect ratio of approximately 3. Similar elongated micelle geometries have been observed using light scattering by Antonietti and co-workers for PS−poly(4-vinylpyridine) diblocks in organic solvents.[13] They attributed their micelle geometries to the conformation and interactions of the solvated PS chains forming the micelle corona.[13]

Due to the fact that the micelles are formed in toluene solutions, direct visualization of the structures using microscopy is complicated. Successful imaging of other elongated micelle systems has relied on cryogenic transmission electron microscopy,[20−22,56] which generally requires aqueous solutions. We are currently exploring possibilities for directly imaging this system.

Finally, we must also suggest that it is possible that elongated micelles coexist with spherical micelles. SANS studies have shown two geometries of micelles can coexist, including the coexistence of spheres and rods[57,58] and spheres and disks.[59] The coexistence of two micelle geometries can be likened to the coexistence of free polymer chains and spherical micelles and can be predicted as a second transition at a given micelle concentration (i.e., critical micelle concentration, cmc).[60] Our observation of a single τ in the DLS studies implies that any coexisting spheres must be in very low volume fraction. Also, the single τ is consistent with micelles of the level of anisotropy we report; more elongated micelles of higher aspect ratio would lead to additional features in the DLS data.

III.4. Solubilizing Small Molecules within Micelles. Micelles have demonstrated the capacity to partition small molecules that are incompatible with the solvent environment within their cores. Many potential applications of block copolymer micelles involve the solubilization of small molecules within their structures; thus a fundamental understanding of the governing relationships could impact their utility. The partitioning of small molecules to the core of a micelle has been studied both theoretically[61−63] and experimentally.[43,49,51,64−69] A series of studies on lecithin (a small-molecule surfactant) in isooctane explored the water-induced growth of the cylindrical reverse micelles.[64−66] Through systematic light and neutron scattering experiments, the structure of the long and flexible polymer-like micelles was investigated in the presence of small amounts of water.[64,66] Rheological experiments explored the dynamic behavior of the transient networks formed by entangled polymer-like micelles.[65] All these studies supported the conclusion that the addition of water to the surfactant system induced growth in the length of the polymer-like micelles, thus creating dynamic behavior likened to the viscoelastic behavior found in polymeric systems. In a scattering study of spherical micelles, Cogan and co-workers found that small amounts of water greatly affected both the size and aggregation number of the micelles of PS−PEO block copolymers.[49,51,69] Using ^{1}H NMR chemical shifts, Eisenberg et al. explored the distribution of water in block ionomer micelles in toluene.[67,68] Small molecules besides water have been solubilized in micelles, including the encapsulation of fullerenes[70] and enzymes.[5,6] Antonietti and co-workers have prepared palladium colloids for catalysis by using containment within PS−poly-4-vinylpyridine copolymer micelles.[3]

In our system, we believe that the trace amounts of water present may aid in the copolymer micellization. Water may act as a nucleating agent for the formation of micelles or may stabilize the micelle structures once formed; the presence of water in the micelle cores may allow for more efficient packing of the IL blocks.

We assessed the ability of our micelle systems to solubilize small molecules by measuring their water

(55) Kline, S. R. *NIST Center for Neutron Research Internal Report*; National Institute of Standards and Technology: Gaithersburg, MD, 2001.
(56) Zheng, Y.; Won, Y. Y.; Bates, F. S.; Davis, H. T.; Scriven, L. E.; Talmon, Y. *J. Phys. Chem. B* **1999**, *103*, 10331−10334.
(57) Nakano, M.; Matsuoka, H.; Yamaoka, H.; Poppe, A.; Richter, D. *Macromolecules* **1999**, *32*, 697−703.
(58) Bernheim-Groswasser, A.; Wachtel, E.; Talmon, Y. *Langmuir* **2000**, *16*, 4131−4140.
(59) Nakano, M.; Matsumoto, K.; Matsuoka, H.; Yamaoka, H. *Macromolecules* **1999**, *32*, 4023−4029.
(60) May, S.; Ben-Shaul, A. *J. Phys. Chem. B* **2001**, *105*, 630−640.
(61) Cogan, K. A.; Leermakers, F. A. M.; Gast, A. P. *Langmuir* **1992**, *8*, 429−436.
(62) Nagarajan, R. *Polym. Adv. Technol.* **2001**, *12*, 23−43.
(63) Nagarajan, R.; Ganesh, K. *J. Chem. Phys.* **1993**, *98*, 7440−7450.
(64) Schurtenberger, P.; Scartazzini, R.; Magid, L. J.; Leser, M. E.; Luisi, P. L. *J. Phys. Chem.* **1990**, *94*, 3695−3701.
(65) Schurtenberger, P.; Magid, L. J.; Penfold, J.; Heenan, R. *Langmuir* **1990**, *6*, 1800−1803.
(66) Schurtenberger, P.; Cavaco, C. *Langmuir* **1994**, *10*, 100−108.
(67) Khougaz, K.; Gao, Z. S.; Eisenberg, A. *Langmuir* **1997**, *13*, 623−631.
(68) Gao, Z. S.; Desjardins, A.; Eisenberg, A. *Macromolecules* **1992**, *25*, 1300−1303.
(69) Cogan, K. A.; Gast, A. P. *Macromolecules* **1990**, *23*, 745−753.
(70) Chen, X. L.; Jenekhe, S. A. *Langmuir* **1999**, *15*, 8007−8017.

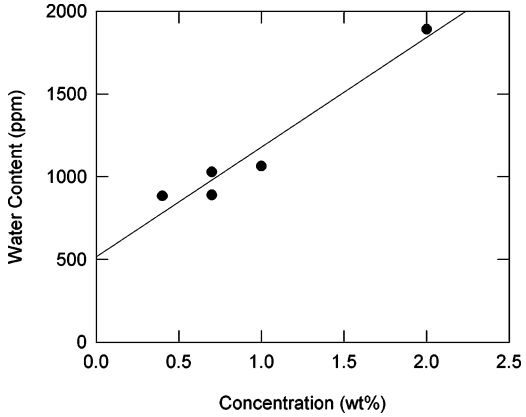

Figure 5. The water content (ppm) is plotted as a function of the PS(198)−IL(111) concentration (wt %). The solid line indicates a least-squares fit to the data.

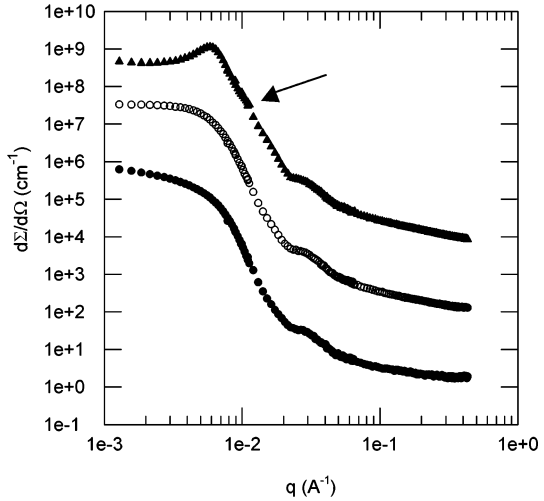

Figure 6. SANS scattering profiles normalized by concentration are shown for PS(198)−IL(111) at 0.7 wt % (closed circles), 5 wt % (open circles), and 20 wt % (closed triangles) in toluene where the 5 wt % and 20% data are offset by multiplicative factors of 10^2 and 10^4, respectively, for clarity. The arrow indicates the shoulder position in the 20 wt % scattering profile. The solvent contribution to these scattering profiles has not been removed but only contributes to the intensity as a uniform background.

uptake. To investigate the capacity of the micelles to contain water, we saturated micelle solutions of PS(198)−IL(111) with water at varying copolymer concentrations (0.4−2.0 wt %). We employed Karl Fischer titration to determine the water content of ambient and saturated copolymer samples as well as toluene. Although water and toluene are not miscible, 510 ppm of water is present in our saturated toluene sample in agreement with the reported solubility limit of water in toluene of 330 ppm.[71] The excess over the saturation value arises from water introduced in the preparation procedures (i.e., trace amounts of water on the glassware) and should be constant throughout the study. Our study of PS(198)−IL(111) shows the water content is linearly related to the concentration of copolymer (Figure 5). We find that about 1−2 water molecules are solubilized within the micelles for every IL repeat unit independent of the copolymer concentrations in the range studied. By extrapolating the linear fit to vanishing copolymer concentration, we obtain the water content of saturated toluene of 520 ppm in excellent agreement with our saturated toluene results. An ambient sample of PS(198)−IL(111) prepared at 2 wt % showed a water content 50 ppm over that of ambient solvent, indicating that some water is present in micelles of samples that have not been explicitly exposed to water. The water could be associated with the copolymer and may be difficult to remove with standard drying procedures. As samples were not prepared in a dry environment, water may come into contact with the sample and solvent through the atmosphere.

Studies of the compatibility of imidazolium functionalities with water have found that the water uptake is a function of both the pendant functionalities on the imidazolium ring structure and the associated counterion.[72,73] When we extrapolate the water content of our BF_4^- copolymer solution to a bulk value (i.e., a concentration of 100%), we find a water content of about 66 000 ppm that is consistent with values reported for other bulk imidazolium structures with BF_4^- counterions of 20 000 and 14 000 ppm.[73]

III.5. Micelle Behavior at Elevated Concentrations. We collected SANS data for PS(198)−IL(111) at three concentrations of 0.7, 5, and 20 wt % in toluene as shown in Figure 6. We see that the shape of the dilute solution scattering profile is due to the micelle form factor. With increased volume fraction, micelles begin to interact with one another and the structure factor contributes to the scattering profile. In Figure 6, we see the features due to the structure factor, including a downturn in the scattering at low q and a peak and shoulder (indicated with the arrow in Figure 6) in the scattering profile at intermediate q. We find these features become more pronounced with an increase in concentration from 5 to 20 wt %, indicating the interactions are enhanced as the volume fraction of micelles increases.

To assess the micelle interactions, we compare the scattering profiles of the concentrated solutions to the dilute solution profile in Figure 6. In the high-q regime, we find that the scattering profiles nearly coincide and are identical in shape at all three concentrations. Hence, the structure factor does not impact this regime of the scattering profile and we conclude that the increase in concentration does not change the structure of the chains within the micelle, and thus we believe there are no dramatic changes to the micelle shape. While we cannot directly obtain the structure factor from the data as it is coupled to the form factor, we can deduce that the features that evolve with concentration in the scattering profiles are due to the structure factor. Clearly the large, low-q peak in the scattering profile at high concentration is due to a peak in the structure factor. Generally speaking, peaks in the structure factor indicate preferred interparticle separation distances (d) which can be approximated as $d \sim 2\pi/q_{max}$. In our profile, the peak due to the structure factor is found at a q-value of 0.006 Å^{-1} indicating an interparticle spacing of about 1000 Å. The shoulder in the profile is subtle but exists at 5 wt % and is more pronounced at 20 wt %, suggesting that it is in fact due to the structure factor. The shoulder begins at a q-value of about 0.01 Å^{-1} and continues to about 0.02 Å^{-1}. This gives an interparticle spacing of about 400−600 Å, roughly corresponding to $R_{g,xs}$, perhaps indicative of the center-to-center distance between two micelles in contact with one another. The distance of 1000 Å is not directly linked to any length scale of the elongated micelle structures, but we can

(71) Smallwood, I. M. *Handbook of Organic Solvent Properties*; Halsted Press: New York, 1996.
(72) Seddon, K. R.; Stark, A.; Torres, M. J. *Pure Appl. Chem.* **2000**, *72*, 2275−2287.
(73) Cammarata, L.; Kazarian, S. G.; Salter, P. A.; Welton, T. *Phys. Chem. Chem. Phys.* **2001**, *3*, 5192−5200.

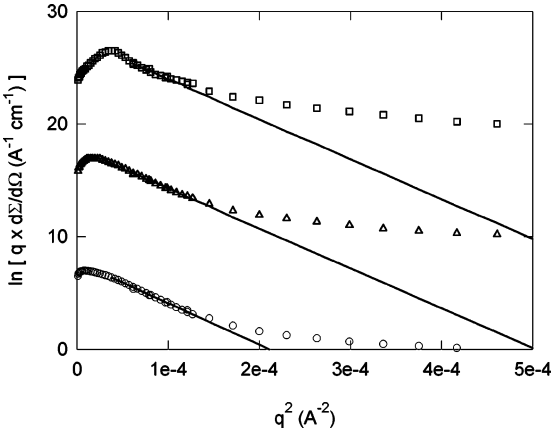

Figure 7. The Kratky−Porod wormlike chain analysis is shown for toluene solutions of PS(198)−IL(111) at 0.7 wt % (open circles), 5 wt % (open triangles), and 20 wt % (open squares). The data are offset for clarity by an additive factor of 10 for 5 wt % and 20 for 20 wt %. The solid lines indicate the linear fits used to obtain the $R_{g,xs}$.

conclude that higher order liquid structure exists in this system of concentrated elongated structures.

While the low-q depression in the scattering profile due to the structure factor disrupts the low-q regime and the bending rod analysis is limited to dilute solutions, we can still apply the Kratky−Porod wormlike chain analysis to the concentrated solutions as shown in Figure 7. We see that while the linear regime is truncated by increasing concentration, we can still obtain linear fits with nearly the same slopes as those observed for the dilute solution. Thus, the $R_{g,xs}$ for these structures is not changed with increasing concentration (271, 266, and 267 Å for 0.7, 5, and 20 wt %, respectively), indicating the micelles must grow either in number or in length to accommodate the additional copolymers in solution, but not in cross-section. This is further evidence that the IL block length dictates the cross-sectional dimension of the micelles.

IV. Conclusions

By building relationships between the properties of a diblock copolymer and its assemblies, we can tailor polymers to achieve desired assembled structures. In our study of this diblock copolymer system, we find that the length of the IL block strongly influences the properties of the copolymer assemblies. The PS−IL copolymers show strong evidence for the formation of elongated micelle systems in dilute toluene solutions in our scattering data analysis. We find that the IL block dictates the micelle geometry and dimensions. Surprisingly, we find that many of the parameters that describe the micelle structures depend linearly on the length of the IL block. This unique relationship between the soluble block and the micelle structure over a range of block ratios is unprecedented in other micelle systems. We also have found that the micelles of these copolymers have the capacity to contain water. We will continue to explore potential applications for these systems that leverage their unique ionic liquid functionality with their ability to contain and sequester small molecules. Future SANS investigations will explore the structures of the micelle core and shell independently by use of selectively deuterated copolymers.

Acknowledgment. We thank Professor Nitash Balsara for use of his DLS instrument and Mr. Timothy J. Rappl for assistance with these experiments. We acknowledge support for this work from the NSF Center for Polymer Interfaces and Macromolecular Assemblies (CPIMA), Grant No. DMR-9808677. We acknowledge the support of the National Institute of Standards and Technology, U.S. Department of Commerce, in providing facilities used in this work. This material is based upon activities supported by the National Science Foundation under Agreement No. DMR-9986442. We thank Institut Laue-Langevin for providing facilities used in this work. A.R.L. thanks the National Institutes of Health for a postdoctoral fellowship (66597-01).

LA0353632